

Urban planning at the heart of increasingly severe East African flood impacts in a warming world

Authors

Joyce Kimutai, *Grantham Institute, Imperial College London, UK*

Clair Barnes, *Grantham Institute, Imperial College London, UK*

Fredrick Masambaya, *Kenya Meteorological Department, Nairobi, Kenya*

Izidine Pinto, *Royal Netherlands Meteorological Institute (KNMI), De Bilt, The Netherlands*

Obed Matundura Ogega, *African Academy of Sciences, Nairobi, Kenya*

Zacharia Mwai, *Kenya Meteorological Department, Nairobi, Kenya*

Hannah Wangari, *Kenya Meteorological Department, Nairobi, Kenya*

Mary Kilavi, *Kenya Meteorological Department, Nairobi, Kenya*

Maja Vahlberg, *Red Cross Red Crescent Climate Centre, The Hague, the Netherlands (based in Umeje/Umeå, Sweden)*

Julie Arrighi, *Red Cross Red Crescent Climate Centre, The Hague, the Netherlands; Faculty of Geo-Information Science and Earth Observation (ITC), University of Twente, Enschede, the Netherlands; Global Disaster Preparedness Center, American Red Cross, Washington DC, USA (based in New York, USA)*

Emmanuel Raju, *Department of Public Health, Global Health Section & Copenhagen Centre for Disaster Research, University of Copenhagen, Denmark*

Nick Baumgart, *Department of Public Health, Global Health Section & Copenhagen Centre for Disaster Research, University of Copenhagen, Denmark*

Friederike Otto, *Grantham Institute, Imperial College London, UK*

Review authors

Mariam Zachariah, *Grantham Institute, Imperial College, London, UK*

Sjoukje Philip, *Royal Netherlands Meteorological Institute (KNMI), De Bilt, The Netherlands*

Roop Singh, *Red Cross Red Crescent Climate Centre, The Hague, the Netherlands (based in New Jersey, USA)*

Eddie Jjemba, *Red Cross Red Crescent Climate Centre, The Hague, the Netherlands (based in Kampala, Uganda)*

Shaban Mawanda, *Red Cross Red Crescent Climate Centre, The Hague, the Netherlands (based in Kampala, Uganda)*

Main findings

- Countries in East Africa have been facing disaster after disaster, including prolonged drought between 2020-23, and multiple episodes of torrential rainfall leading to severe flooding. These disasters combine to create a complex humanitarian emergency that includes displacement, infrastructure loss, food insecurity, health risks, disrupted livelihoods, and overall weakened resilience.
- Rapid urbanisation in cities across East Africa is amplifying flood risks, especially in large informal areas that are located on flood-prone land, lack adequate structural protections from the rains, and whose residents lack resources to recover and rebuild. Land-use changes, including deforestation and conversion to agricultural land are also occurring to different degrees in each of the countries studied, adding to flood risk.
- The East African long rains were observed to show a drying trend towards the end of the 20th century, while climate models projected an increase in heavy rainfall with global warming. While this so-called East Africa Paradox is not as pronounced anymore, with observed precipitation increasing and a new generation of climate models showing weaker or no wettening trend, interpreting observations and climate models is still challenging in this region.
- The observations, independent of the exact region and data product, do not show a long term trend, but instead a drying trend towards the end of 20th century up until around 2008 and a wettening in the last 15 years. Regardless of whether the recent recovery is being enhanced by human-induced climate change, the increased precipitation does bring an increased risk of flooding to the region.
- To understand if human-induced climate change is indeed playing a role, we also assess whether there are wettening or drying trends in the region for the long rains in climate models. While the trends are not statistically significant, they do show a wettening. On average, an event like this has become about twice as likely and 5% more intense in today's climate, representing the effect of 1.2C of global warming.
- Looking at the future, for a climate 2°C warmer than in preindustrial times, models suggest that rainfall intensity and likelihood will increase further.
- We also examined whether the current phase of the El Nino Southern Oscillation or the Indian Ocean Dipole played a role in the intensity and likelihood of the wet March-May rainy season. Both modes of natural climate variability have been found to exhibit a negligible influence on the 2024 long rains in the study region.
- Taking these findings and the known physical relationship that heavy rainfall is expected to increase in a warming world, we conclude that the observed increase in rainfall in the region over the last 15 years is in part driven by human-induced climate change.
- Therefore, investing in flood resilience with future warming is paramount.
- While early warning systems in each of the countries exist and warn of extreme rainfall, there is room to expand the action taken based on warnings to adequately protect people from the rainfall impacts. Social protection programs can fill gaps in instances where it's not possible to avoid all impacts, in order to help people recover their assets and livelihoods after the disaster.
- Disaster preparedness policies, flood preparedness and protection infrastructure, and early warning systems that are in place across Kenya, Tanzania and Burundi are all steps in the right direction, but must be integrated and implemented at scale in order to reduce impacts

1 Introduction

Intense and recurrent extreme weather and climate events in East Africa ([Kilavi et al., 2018](#); [Kimutai et al., 2022](#); [Palmer et al., 2023](#); [Liebmann et al., 2014](#); [Philippon et al., 2015](#); [Hoell et al., 2017](#); [Funk et al., 2018](#)) continue to wreck developmental gains and subject hardship for communities across the region. In 2011 ([Lott et al., 2013](#)), 2016-2017 ([Uhe et al., 2018](#)) and 2020-2023 ([WWA, 2023](#); Kimutai et al., under review), prolonged drought conditions resulted in widespread impacts to humans, including crop and harvest losses, livestock deaths, hunger, and malnutrition. In March-April-May (MAM) 2012, 2016 and 2018 ([Kimutai et al., 2022](#)) and October-November-December (OND) 2019 ([FEWSNET, 2020](#); [Wainwright et al., 2020](#)) and 2023 ([WWA, 2023](#)) the region experienced several heavy precipitation events with devastating impacts on agriculture, infrastructure, settlements, property, and life. In March-April 2024, the region experienced devastating flooding causing human deaths, destroying infrastructure and crops and killing livestock and wildlife. In April 2024, floods killed over 200 people and displaced over 150,000 people in Kenya. A dam burst on 29 April in Nakuru County killing at least 50 people, among them 17 children. By the end of April, over 4,824 livestock had been lost, 27,717 acres of croplands damaged with 264 small businesses and 24 schools adversely affected. Schools and businesses remained closed across the country ([OCHA, 2024](#)). Several main roads were rendered impassable. The floods also destroyed about 60 health facilities across 11 counties. In the same month, very heavy rainfall was recorded in Nairobi and the Central parts of Kenya, with the Kenya Meteorological Department issuing heavy rainfall advisories on the 1st, 13th and 18th ([KMD, 2024](#); [The Star, 2024](#)). These downpours caused serious flooding, especially near riparian areas and also downstream of River Athi and River Tana; the Seven Forks dams overflowed, exacerbating the dire situation in Garissa and Tana river Counties also referred to as lower Tana basin. In the western part of the country the Yala river in the Yala basin broke its banks and caused massive flooding in the basin, while it was also reported that the backflow from Lake Victoria caused flooding in lower Nzoia which comprises Bunyala sub county. Heavy rainfall is expected to persist throughout May ([KMD, 2024](#); [Kenyans, 2024](#)).

In Tanzania, weeks of rainfall in March and April resulted in 155 human deaths and a further 200,000 adversely affected, as well as massive damage, with floods sweeping away houses, roads, bridges, schools, and farmland ([CBS News, 2024](#); [AP, 2024](#)). The regions highly impacted by the heavy rains include the coastal region and the capital Dar es Salaam, mountain regions of Hanang in northern Tanzania and along Rufiji river and the islands of Zanzibar and Pemba ([TMA, 2024](#); [IFRC, 2024](#); [BBC, 2024](#)). Tanzania Meteorological Authority (TMA) continued to issue advisory alerts of possible storm surge and heavy rainfall along the coast and the Island regions as Tropical Cyclone Hidaya progressed towards their coast ([TMA, 2024](#)). Hidaya made landfall on Tanzania's coastline on May 4, 2024, with high rainfall recorded in Mtwara, Lindi, and Morogoro regions ([EastAfrican, 2024](#)). In Burundi, more than 96,000 people had been displaced by floods by the end of April ([Al Jazeera, 2024](#)). The most affected regions were areas around Lake Tanganyika, including the capital Bujumbura ([Africanews, 2024](#)). IOM (International Organization for Migration) supported relocation of people to safer and higher ground areas and distributed emergency goods like blankets, cooking utensils, solar lamps, and safety kits to more than 5,000 people ([IOM, 2024](#)).

1.1 Event Definition

The impacted areas were affected by a series of heavy rainfall events, rather than a single heavy downpour. This is typical of the long rains: the temporal distribution of rainfall in MAM generally comprises successive 5-day to 10-day wet spells, punctuated by dry spells (e.g. [Camberlin & Okoola, 2003](#)). We therefore look at the maximum accumulated rainfall over a 30-day period (RX30day) during the months of March-May, averaged over a large region that covers the flooded areas around Lakes Victoria and Tanganyika, in the Central Highlands of Kenya, and in low-lying and coastal Tanzania (outlined in red in Figure 1.1). We note that at the time of writing, data were only available until the end of April 2024, and therefore the wettest 30-day period in 2024 was identified on this basis, although the heavy rain is expected to continue during May. In four of the datasets, the period from March 27th-April 25th (plus one day on either side) is identified as the wettest 30-day period; in MSWEP the wettest period in this region ended on April 21st. All of the gridded data products considered show similar spatial patterns, with very high rainfall accumulations over the central highlands and southeast Tanzania in particular.

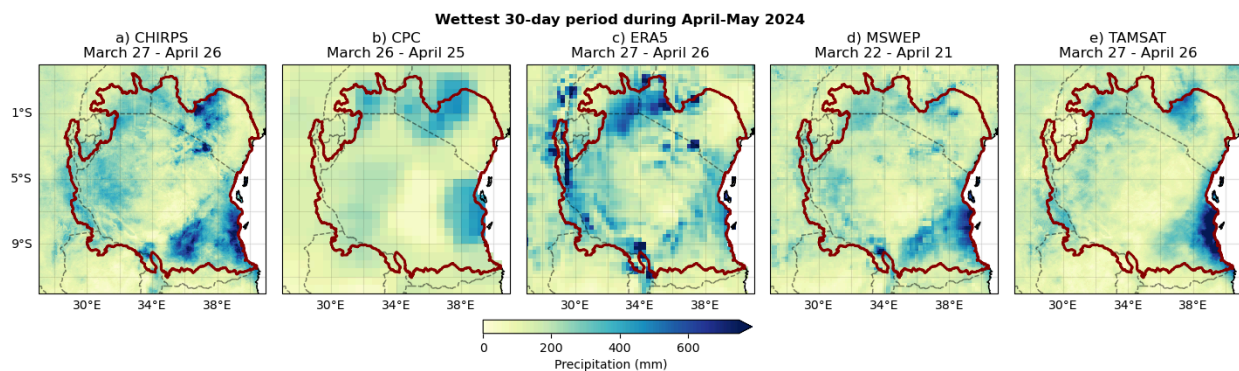


Figure 1.1: Map of accumulated precipitation during the wettest 30-day period over the study region (outlined in red) during April-May 2024, in five different gridded data products: (a) CHIRPS; (b) CPC; (c) ERA5; (d) MSWEP; (e) TAMSAT.

1.2 Drivers of the Long Rains

Precipitation over East Africa is characterised by high seasonal and interannual variability, driven by various local and remote factors. Equatorial East Africa experiences a bimodal rainfall distribution: the main rainfall season, ‘long rains’ occurs in March-April-May (MAM) while the ‘short rains’ season occurs in October-November-December (OND). Seasonal rainfall is controlled by the position and movement of the Intertropical Convergence zone (ITCZ) at the equator as it transitions between 15°N and 15°S. The three main moisture sources for rainfall are Lake Victoria, Indian Ocean, and the humid layer of the Congo air mass. Rainfall variability is modulated by the interaction between the ITCZ and perturbations in the global and regional circulation, as well as changes in mesoscale systems initiated by land surface heterogeneity induced by vegetation characteristics, large lakes and topography. The contrasting topographical settings in the region induce widespread dynamic effects and sub-synoptic disturbances through mesoscale circulation systems. Notably, the highlands perturb uniform flow and create rain shadows as they block the flow of moist air mass either from the Congo basin or the Indian Ocean ([Ogwang et al., 2014](#)). Mesoscale flows form a coupling between Lake Victoria and the surrounding mountains, leading to storm formation on highland regions during the afternoon, and over the

lake at night as a result of lake-land thermal contrast (land and sea breezes) ([Chamberlain et al., 2014](#); [Dyer and Washington, 2021](#); [Thiery et al., 2016](#)). Large-scale synoptic conditions in MAM are largely governed by the interplay of pressure differences in the sub-tropical high-pressure systems. Changes in sea level pressure over the Indian and Atlantic oceans control the zonal advection of moisture across the region. The presence of tropical cyclones in the southwest Indian Ocean have been associated with enhanced anomalous westerly flow over many parts of Eastern Africa ([Kebacho, 2022](#)). The influence of tropical cyclones on the region's weather depends on their relative position and intensity. Generally, they tend to interfere with the normal easterly low-level flow of winds. In MAM 2018, for instance, the anomalous cyclonic circulation observed over the southwest Indian Ocean with a corresponding strengthened St. Helena High was a significant feature of the widespread lower tropospheric westerlies across East Africa ([Kilavi et al., 2018](#); [Finney et al., 2019](#)). Westerly flow favours the influx of moisture from both the Congo basin, and the push and positioning of the meridional arm of the ITCZ over East Africa. Other drivers for MAM rainfall are Madden Julian Oscillation and the Indian Ocean Dipole (IOD). Most studies link MJO to intra-seasonal spells of enhanced or suppressed MAM rainfall in East Africa, depending on the MJO phase. Years of high MJO amplitude (phases 2–4) are characterised by earlier onsets and higher seasonal amounts ([Pohl & Camberlin, 2006](#)). MJO was found to be in an active phase (with the main centre of enhanced convection concentrated over the western Indian Ocean) during the high rainfall events of 1981, 1990, 1997, 2010, 2013, 2016 and 2018 ([Philippon et al. 2015](#); [Kilavi et al., 2018](#)). Warmer sea surface temperature (SST) anomalies in the western Indian Ocean, partially controlled by the IOD, is known to contribute to enhanced MAM rains in equatorial Eastern Africa ([Vellinga et al., 2018](#)). Under climate change and global warming, more variability and extremism in east Africa's rainfall patterns is expected ([Ogega et al., 2023](#), [Gebrechorkos et al., 2023](#)).

1.3 Effect of climate change on the region and the East African climate paradox

[Kimutai et al. \(2022\)](#) conducted a study to investigate the impact of human-induced climate change on the intensity of heavy precipitation events during March-April-May in 2012, 2016, and 2018 over different regions in Kenya. Using three distinct experiments with independent event-attribution methodologies, the study found a potential emerging signal of human influence on increased rainfall events. However, this influence cannot yet be definitively attributed to human-induced climate change.

Observations and model projections over East Africa have been known to disagree, with observations showing a drying, especially from the mid-1990s to the first decade of 21st century, and projections showing a wetting trend, described as the “East Africa Paradox” ([Rowell et al., 2015](#)). Studies have explored some hypotheses to explain this phenomenon. [Tierney et al. \(2015\)](#) argued that the projected increase in rainfall mainly occurs during the short rains (OND) season and not much in the MAM season, in response to large-scale weakening of the Walker circulation and simulated El-Niño-like shifts majorly occurring during the short rains. [Giannini et al. \(2018\)](#) argued that the substantial biases in simulations of the regional climate, and discrepancy in the modelled versus observed tropical Pacific and Indian SST trends limits the confidence and reliance in projections of future increase in rainfall in East Africa. The study shows that it is unclear whether the current cooling of the tropical eastern Pacific is due to internal variability alone or partly attributable to evolving La Niña-like conditions due to increasing GHGs in the atmosphere. They pointed out the limitation of models in simulating rainfall associated with the complex mesocycle process influenced by East African topography in advection of moisture from the Indian Ocean

and Congo Basin. Similarly, [Batté & Déqué \(2011\)](#) agrees that the paradox can partly be explained by a limited understanding of the complexity of the interactions between local, regional, and large-scale processes in the regions making model simulations less robust compared to other regions like extra tropics. [Wainwright et al. \(2019\)](#) shows that more recently the paradox has been associated with shorter rather than less intense rains in the MAM season, with the drying driven by SST and pressure gradient anomalies over the Arabian seas. Overall, the mechanisms that drive the paradox remain unclear. However, observations show a recovery in the drying trend from around 2010.

On future projections, the IPCC 6th Assessment report ([IPCC, 2021](#)) concludes that heavy rainfall is projected to increase over Eastern Africa but with considerable variability between seasons and models used. In north-east and central east Africa, extreme precipitation intensity is projected to increase across CMIP5, CMIP6 and CORDEX-CORE (high confidence) in most areas annually but for the long rains in particular, trends only emerge with high warming levels ([Seneviratne et al., 2021](#), [Ongoma et al., 2017](#)).

2 Data and methods

2.1 Observational data

We utilise five daily gridded observational datasets:

(i) CHIRPS (Climate Hazards Group InfraRed Precipitation with Station data; [Funk et al., 2015b](#)), a daily dataset developed by the UC Santa Barbara Climate Hazards Group, incorporating satellite data, infrared Cold Cloud Duration (CCD) estimates and blended station data. Daily data are available from 1981-present at 0.05° resolution from 60S to 60N.

(ii) The CPC Global Unified Daily Gridded data, which covers the globe at 0.5° resolution, for the period 1979-present. Data are available from [NOAA](#).

(iii) The ERA5 reanalysis product ([Hersbach et al., 2020](#)) produced by the European Centre for Medium-Range Weather Forecasts. This product covers the globe at 0.25° resolution, starting in 1950. The variables from ERA5 are not directly assimilated, but are generated by atmospheric components of the Integrated Forecast System (IFS) modelling system. Reanalysis data is available until the end of April 2024.

(iv) MSWEP (Multi-Source Weighted-Ensemble Precipitation) v2.8 dataset (updated from [Beck et al., 2019](#)), which combines gauge, satellite, and reanalysis-based data. Data is available at 3-hourly intervals from 1979 to ~3 hours from real-time, and at 0.1° spatial resolution globally. Daily-resolution data is used in this study.

(v) TAMSAT (Tropical Applications of Meteorology using SATellite and ground based observations, [Maidment et al., 2017](#)), a daily rainfall dataset based on using high-resolution thermal-infrared

observations to identify precipitating clouds. Daily rainfall data are available at $0.0375^\circ \times 0.0375^\circ$ spatial resolution over the African continent from 1983 to the present.

As a measure of anthropogenic climate change, we use the (low-pass filtered) global mean surface temperature (GMST), where GMST is taken from the National Aeronautics and Space Administration (NASA) Goddard Institute for Space Science (GISS) surface temperature analysis (GISTEMP, [Hansen et al., 2010](#) and [Lenssen et al., 2019](#)).

The detrended Niño3.4 index is computed from [NOAA's ERSST v.5](#) sea surface temperatures, by subtracting the mean tropical SST (20S-20N) from the mean SST over the Niño3.4 region (5S-5N, 170W-120W) ([van Oldenborgh et al., 2021](#)). Time series of the observed [IOD](#) derived from the ERSST dataset were obtained from [KNMI's Climate Explorer tool](#).

2.2 Model and experiment descriptions

We use three multi-model ensembles from climate modelling experiments using different framings ([Philip et al., 2020](#)): High-resolution sea surface temperature (SST)-driven global circulation models, regional climate models, and low-resolution coupled global circulation models.

1. HighResMIP SST-forced model ensemble ([Haarsma et al., 2016](#)), which spans from 1950 to 2050. The SST and sea ice forcings for the period 1950-2014 are obtained from the $0.25^\circ \times 0.25^\circ$ Hadley Centre Global Sea Ice and Sea Surface Temperature dataset that have undergone area-weighted regridding to match the climate model resolution. For the 'future' time period (2015-2050), SST/sea-ice data are derived from RCP8.5 (CMIP5) data, and combined with greenhouse gas forcings from SSP5-8.5 (CMIP6) simulations (see Section 3.3 of [Haarsma et al., 2016](#) for further details).
2. Coordinated Regional Climate Downscaling Experiment (CORDEX)-Africa Domain (AFR-CORDEX) with 0.44° resolution ([Giorgi et al., 2009](#); Nikulin et al., 2012) comprising 11 simulations resulting from pairings of Global Climate Models (GCMs) and Regional Climate Models (RCMs). These simulations are composed of historical simulations from 1950 up to 2005, and extended to the year 2100 using the RCP8.5 scenario.
3. We use 17 simulations from the CMIP6 ensemble ([Eyring et al., 2016](#)). For all simulations, the period 1850 to 2015 is based on historical simulations, while the SSP5-8.5 scenario is used for the remainder of the 21st century.

2.3 Statistical methods

Methods for observational and model analysis and for model evaluation and synthesis are used according to the World Weather Attribution Protocol, described in [Philip et al., \(2020\)](#), with supporting details found

in [van Oldenborgh et al., \(2021\)](#), [Ciavarella et al., \(2021\)](#) and [here](#). The key steps, presented in sections 3-6, are: (3) trend estimation from observations; (4) model validation; (5) multi-method multi-model attribution; and (6) synthesis of the attribution statement.

In this report we analyse time series of March-May maxima of 30-day accumulated precipitation (RX30day) over the study region outlined in Figure 1.1; precipitation is averaged over the region before the 30-day maxima are identified.

A nonstationary generalised extreme value (GEV) distribution is used to model the variable. The distribution is assumed to scale exponentially with the global mean surface temperature (GMST), with the dispersion (the ratio between the standard deviation and the mean) remaining constant over time. The parameters of the statistical model are estimated using maximum likelihood. For each time series we calculate the return periods, probability ratio (PR; the factor-change in the event's probability) and change in intensity of the event under study for the 2024 GMST and for 1.2C cooler GMST: this allows us to compare the climate of now and of the preindustrial past (1850-1900, based on the [Global Warming Index](#)).

3. Observational analysis

3.1 Analysis of gridded data

Figure 3.1 shows the time series of MAM RX30day over the study region in each of the five gridded data products listed in Section 2.1. All of the data products exhibit similar behaviour over this region: stable or slowly decreasing rainfall prior to the mid-1990s, followed by a rapid decline from around 1997-2008 and a period of low rainfall with low interannual variability (shaded in yellow), and recovery thereafter. This observed pattern is part of a phenomenon known as the East African Paradox ([Rowell et al., 2015](#)). While the Paradox is usually defined with reference to the MAM season as a whole, and is not expected to affect the intensity of short-duration rainfall over the region, the effect on the accumulated precipitation during the wettest month of the season is clear in Figure 3.1. This phenomenon is observed across all parts of the study region and in all of the gridded data products tested (Figures A1-A2). The nature of the trend prior to this decline is not clear due to the short length of most of the available time series; although the longer ERA5 dataset shows a decrease in RX30day since 1950, reanalysis has been shown to be unreliable prior to the satellite era for precipitation in this region ([Nicholson & Klotter, 2021](#)).

Without a full understanding (and therefore a statistical model) of the dynamical mechanisms behind the decline and subsequent recovery of MAM precipitation in this region, it is not currently possible to isolate and identify the effect of climate change on the accumulated rainfall in this region.

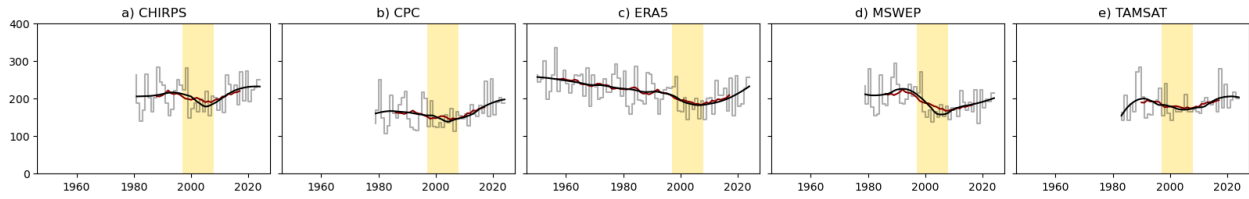


Figure 3.1: Time series of MAM RX30day over the study region in five gridded data products: (a) CHIRPS; (b) CPC; (c) ERA5; (d) MSWEP; (e) TAMSAT. The thick black line is a loess (local regression) curve; the dark red line is a 15-year rolling mean. The shaded region indicates the period from 1997-2008.

3.2 Influence of modes of natural variability

The El-Niño Southern Oscillation (ENSO) is known to play a part in precipitation in this region at certain times of the year. Figure 3.2 plots the RX30day values against the detrended Niño3.4 index (see Section 2.1) averaged over the preceding December-February period, an index chosen to capture the extrema of the ENSO in a typical year. While we do not perform any formal statistical tests due to the difficulty of building a reliable statistical model for this data as described above, a line of best fit indicates that lower RX30day precipitation is expected following a positive ENSO phase: we therefore conclude that it is unlikely that the current declining El Niño phase enhanced the heavy rainfall in this region in recent weeks. Similarly, Figure 3.3 shows the RX30day values against the MAM mean of the Indian Ocean Dipole (IOD); the relationship between the two is very weak (e.g. [Palmer et al., 2023](#)), with positive IOD states associated with slightly lower values of RX30day, and there is no evidence that the current IOD state enhanced the heavy rainfall.

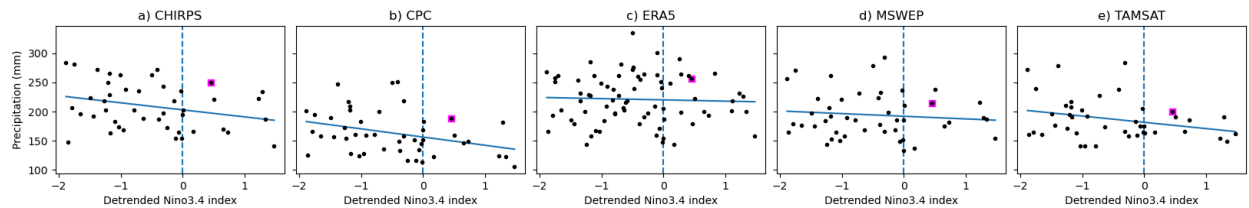


Figure 3.2: Plot of MAM RX30day over the study region in five gridded data products against detrended Niño3.4 index averaged over the preceding December-February: (a) CHIRPS; (b) CPC; (c) ERA5; (d) MSWEP; (e) TAMSAT. The pink marker indicates the 2024 event; the blue line is the line of least-squares best fit.

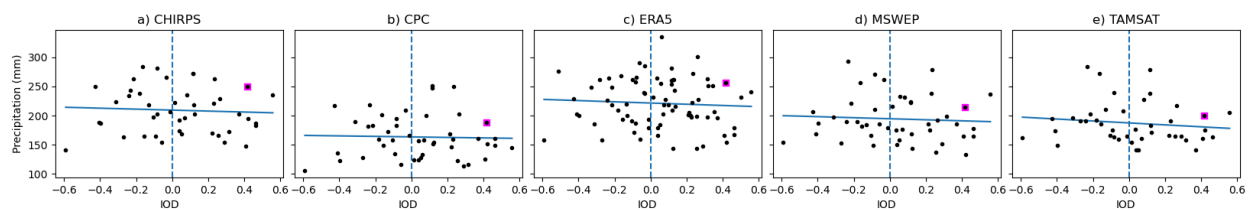


Figure 3.3: Plot of MAM RX30day over the study region in five gridded data products against IOD index averaged over March-May: (a) CHIRPS; (b) CPC; (c) ERA5; (d) MSWEP; (e) TAMSAT. The pink marker indicates the 2024 event; the blue line is the line of least-squares best fit.

4 Model evaluation

The second step in the WWA protocol is to evaluate climate models to understand how well they are able to replicate the observed distribution of precipitation in the region of interest, in order to select models to include in the overall synthesis of the results. Typically, the climate models are evaluated against the gridded observational data products for their ability to capture the distribution of the variable of interest (here, RX30day). However, because of the difficulty of fitting a statistical model to the observed trends in 30-day accumulated precipitation in this region, this step of the evaluation cannot be carried out. Models are evaluated in terms of how well they represent the spatial and seasonal patterns of MAM precipitation over the region. In addition, for the HighResMIP ensemble only, which is driven by observed SSTs prior to 2015, we note whether the model exhibits the expected dip in rainfall from 1997-2008 (labelled ‘EAP decline’ in the table); plots of the associated time series are shown in Figure A3 in the Appendix. Almost half of the HighResMIP runs evaluated display a similar drying to that seen in the observations. In the tables below we show the results of this model evaluation. If the model is ‘good’ for all criteria, we give it an overall rating of ‘good’. We rate the model as ‘reasonable’ or ‘bad’, if it is rated ‘reasonable’ or ‘bad’, respectively, for at least one criterion. For each collection of runs, if more than five models achieve a ‘good’ evaluation overall, then only these models are included in the attribution; if five models or fewer achieve this, then models deemed ‘reasonable’ are also included. Most of the HighResMIP models were evaluated as capturing the seasonal cycle and spatial pattern of MAM precipitation well over this region (Figures A4-A5), but the regional models tended to underestimate the MAM seasonal peak and generally did not reflect the observed spatial distribution of precipitation (Figures A6-A7). The lower-resolution CMIP6 models are unable to capture the topographic variations in the region, but most tend to capture the bimodal seasonality (Figures A8-A9). As a result, models deemed ‘good’ or ‘reasonable’ were included in the final analysis. Where more than one version of the same model passed the evaluation, only the highest-resolution realisation was retained for the synthesis.

Table 4.1: Evaluation of the HighResMIP models considered for attribution of R30day-MAM over the study region. For each model, we evaluate whether the models accurately reflect the seasonal cycle and spatial pattern of MAM precipitation in this region; for HighResMIP, we also assess whether the decline in MAM precipitation in the early 21st century is represented. The overall evaluation is shown in the right-hand column.

Models	Seasonal cycle	Spatial pattern	EAP decline?	Conclusion
CMCC-CM2-HR4	good	good	n	good
CMCC-CM2-VHR4	good	good	y	good
EC-Earth3P-HR	good	good	y	good
EC-Earth3P	good	good	y	good
FGOALS-f3-H	good	good	y	good
FGOALS-f3-L	reasonable	good	n	reasonable
HadGEM3-GC31-HM	good	good	y	good
HadGEM3-GC31-LM	good	bad	y	bad

HadGEM3-GC31-MM	good	good	y	good
HiRAM-SIT-HR	good	good	y	good
HiRAM-SIT-LR	good	good	y	good
MPI-ESM1-2-HR	good	bad	n	bad
MPI-ESM1-2-XR	good	bad	n	bad
MRI-AGCM3-2-H	good	good	y	good
MRI-AGCM3-2-S	good	bad	n	bad
NICAM16-7S	good	reasonable	n	reasonable
NICAM16-8S	good	reasonable	n	reasonable

Table 4.2: Evaluation of the CORDEX AFR-44 models considered for attribution of R30day-MAM over the study region. For each model, we evaluate whether the models accurately reflect the seasonal cycle and spatial pattern of MAM precipitation in this region. The overall evaluation is shown in the right-hand column.

Models	Seasonal cycle	Spatial pattern	Conclusion
CanESM2_CanRCM4	bad	reasonable	bad
CanESM2_RCA4	reasonable	bad	bad
CNRM-CM5_CCLM4-8-17	bad	reasonable	bad
CNRM-CM5_RCA4	bad	bad	bad
CSIRO-Mk3-6-0_RCA4	good	bad	bad
EC-EARTH_RACMO22T	reasonable	reasonable	reasonable
EC-EARTH_RCA4	bad	bad	bad
GFDL-ESM2M_RCA4	bad	bad	bad
HadGEM2-ES_CCLM4-8-17	bad	reasonable	bad
HadGEM2-ES_RACMO22T	reasonable	bad	bad
HadGEM2-ES_RCA4	reasonable	bad	bad
IPSL-CM5A-MR_RCA4	good	bad	bad
MIROC5_RCA4	good	bad	bad
MPI-ESM-LR_CCLM4-8-17	bad	reasonable	bad
MPI-ESM-LR_RCA4	good	bad	bad
MPI-ESM-LR_REMO2009	good	reasonable	reasonable
NorESM1-M_RCA4	good	bad	bad

Table 4.3: Evaluation of the CMIP6 models considered for attribution of R30day-MAM over the study region. For each model, we evaluate whether the models accurately reflect the seasonal cycle and spatial pattern of MAM precipitation in this region. The overall evaluation is shown in the right-hand column.

Models	Seasonal cycle	Spatial pattern	Conclusion	Note
ACCESS-CM2_r1i1p1f1	bad	reasonable	bad	
ACCESS-ESM1-5_r1i1p1f1	bad	reasonable	bad	
CanESM5_r1i1p1f1	reasonable	reasonable	reasonable	

CMCC-ESM2_r1i1p1f1	reasonable	reasonable	reasonable	
CNRM-CM6-1_r1i1p1f2	reasonable	reasonable	reasonable	Only HR version included in synthesis
CNRM-CM6-1-HR_r1i1p1f2	reasonable	reasonable	reasonable	
EC-Earth3_r1i1p1f1	bad	good	bad	
EC-Earth3-Veg_r1i1p1f1	bad	good	bad	
EC-Earth3-Veg-LR_r1i1p1f1	bad	good	bad	
FGOALS-g3_r1i1p1f1	bad	bad	bad	
INM-CM4-8_r1i1p1f1	reasonable	reasonable	reasonable	
INM-CM5-0_r1i1p1f1	good	reasonable	reasonable	
IPSL-CM6A-LR_r1i1p1f1	good	reasonable	reasonable	
MIROC6_r1i1p1f1	reasonable	bad	bad	
MPI-ESM1-2-HR_r1i1p1f1	bad	reasonable	bad	
MPI-ESM1-2-LR_r1i1p1f1	bad	reasonable	bad	
MRI-ESM2-0_r1i1p1f1	bad	reasonable	bad	
NorESM2-LM_r1i1p1f1	good	reasonable	reasonable	Only MM version included in synthesis
NorESM2-MM_r1i1p1f1	good	reasonable	reasonable	
TaiESM1_r1i1p1f1	bad	bad	bad	

5 Multi-method multi-model attribution

As discussed above, the dynamically-driven change in the distribution of RX30day in the study region makes it impossible to fit a statistical distribution to either the observations or the SST-driven HighResMIP runs, which exhibit the same behaviour. However, we do not expect this phenomenon to occur in coupled climate models, and so we fit a nonstationary GEV to the climate model data following the standard WWA protocol (Section 2.3) in order to understand the simulated trends in RX30day in the study region. Table 5.1 shows probability ratios (PR) and relative changes in intensity (ΔI) for those models that passed the evaluation described in Section 4, for a moderately extreme 10-year event.

Table 5.1: Event magnitude, probability ratio and change in intensity for 10-year RX30day over the study region for each model that passed evaluation: (a) from the preindustrial climate to the present and (b) from the present to 2°C above pre industrial temperatures.

Model	10-year event (mm)	(a) -1.2C vs present		(b) Present vs +0.8C	
		Probability ratio	Change in intensity (%)	Probability ratio	Change in intensity (%)
EC-EARTH_RACMO22T	165	1.4 (0.47 ... 5.0)	2.8 (-6.6 ... 13)	1.3 (0.84 ... 2.0)	2.1 (-1.4 ... 5.5)
MPI-ESM-LR_REMO2009	152	0.35 (0.11 ... 0.87)	-13 (-23 ... -1.8)	0.62 (0.30 ... 0.94)	-5.6 (-11 ... -0.8)
CanESM5_r1i1p1f1	301	3.3 (1.6 ... 7.4)	11 (3.0 ... 20)	1.8 (1.6 ... 2.1)	7.0 (4.5 ... 9.3)
CMCC-ESM2_r1i1p1f1	237	3.3 (1.6 ... 11)	11 (4.4 ... 18)	1.6 (1.2 ... 2.3)	4.7 (2.1 ... 7.8)
CNRM-CM6-1-HR_r1i1p1f2	173	0.88 (0.23 ... 1.9)	-1.4 (-11 ... 8.8)	1.0 (0.68 ... 1.3)	0.57 (-3.6 ... 4.2)

INM-CM4-8_rli1p1f1	327	4.6 (1.7 ... 15)	11 (3.3 ... 19)	1.7 (1.2 ... 2.3)	3.7 (1.1 ... 6.2)
INM-CM5-0_rli1p1f1	311	3.7 (1.7 ... 9.5)	15 (3.9 ... 26)	2.0 (1.6 ... 2.5)	8.8 (5.5 ... 12)
IPSL-CM6A-LR_rli1p1f1	270	1.6 (0.76 ... 3.4)	3.5 (-1.8 ... 9.3)	1.4 (1.1 ... 1.7)	2.3 (0.64 ... 4.1)
NorESM2-MM_rli1p1f1	273	1.7 (0.53 ... 8.9)	5.3 (-4.6 ... 21)	1.5 (0.93 ... 2.0)	4.3 (-0.68 ... 8.8)

6 Hazard synthesis

As discussed above, it is not currently feasible to evaluate the long-term influence of anthropogenic climate change on RX30day during the MAM Long Rains, due to the effect of dynamical drivers that are not easily captured in a statistical model. However, given the fact that an increase in the intensity of RX30day has been observed in recent decades (Section 3.1), it is useful to understand whether climate models consistently project a wetting or drying trend in the future. While we do not expect coupled models to represent the drier period if it was dynamically driven as discussed in Section 1.2, these models should nevertheless show a wetting trend if the wetting observed in the last 15 years is, in part, driven by human-induced climate change. The SST-driven HighResMIP runs exhibit similar behaviour to the observations (Figure A3). This means they cannot be used in trend evaluation although they represent spatial and seasonal patterns of precipitation in this region well. This corroborates the hypothesis that the drying at the end of the 20th century and up to 2008 is indeed driven by the specific SST patterns. As expected, the short-term decline does not appear in the CORDEX and CMIP6 coupled runs, which are not constrained by observed SST patterns. For these model runs it is therefore reasonable to fit a linear model that depends on the GMST of the driving GCM as described in Section 2.3., to investigate whether there is any evidence of a trend in RX30day during the MAM rains in this region, in the past as well as under future warming.

We show the results of this in the red bars in Figures 6.1 (for the change from the preindustrial climate to present day) and 6.2 (for the further projected change from the present day to the future). The estimated change in likelihood of what is currently a 1-in-10-year event, and the relative change in intensity of a 1-in-10-year event, are shown for each model that passed model evaluation. The best estimate for each model is marked with a black triangle. A term to account for intermodel spread is added in quadrature to the natural variability of the models: this is shown in the figures as white boxes around the light red bars. The dark red bar shows the model average, consisting of a weighted mean using the (uncorrelated) uncertainties due to natural variability plus the term representing intermodel spread (the white bars). The majority of the models indicate a wetting trend in this region, with only one of the nine indicating a significant drying trend. The weighted mean (dark red box) indicates an overall wetting trend, although it is not statistically significant: similar events are estimated to be around twice as likely now as in preindustrial times (95% confidence interval: 0.5 - 7.6 times as likely), and around 5% more intense (95% confidence interval: 7% less to 20% more intense). In a world with an additional 0.8°C of warming, similar events are estimated to be 1.4 times more likely than in the current climate (95% confidence interval: 0.8 - 2.6 times as likely) and 3% more intense (95% confidence interval: 4% less to 11% more intense). While these results are not statistically significant, we note that the wetting trend in this region is simulated fairly consistently by the CMIP6 models (Figure A10).

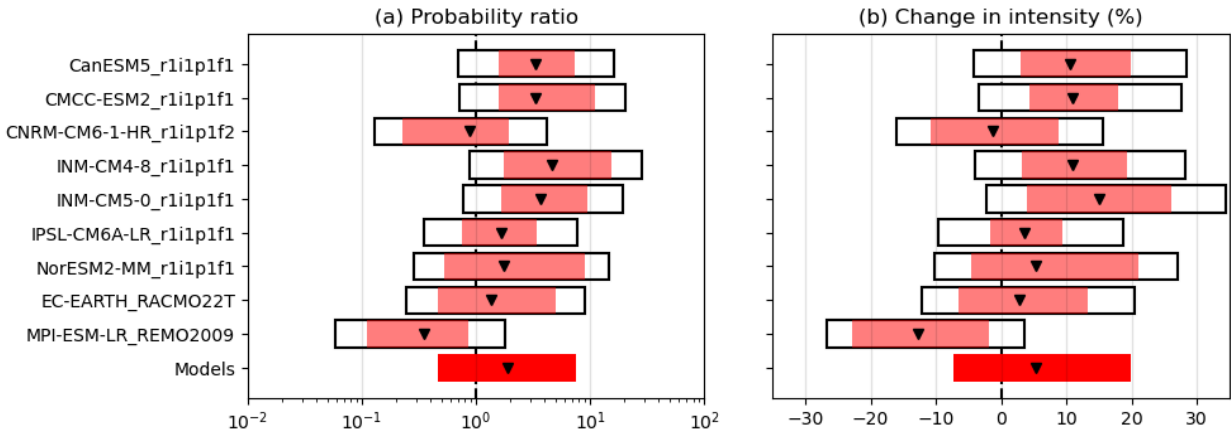


Figure 6.1: Synthesis of (a) probability ratios and (b) relative intensity changes of RX30day over the study region in the 2024 climate and a 1.2°C cooler climate, for all models that were judged ‘reasonable’ or ‘good’ in the model evaluation step. Details of how to interpret the synthesis plots are given in the text.

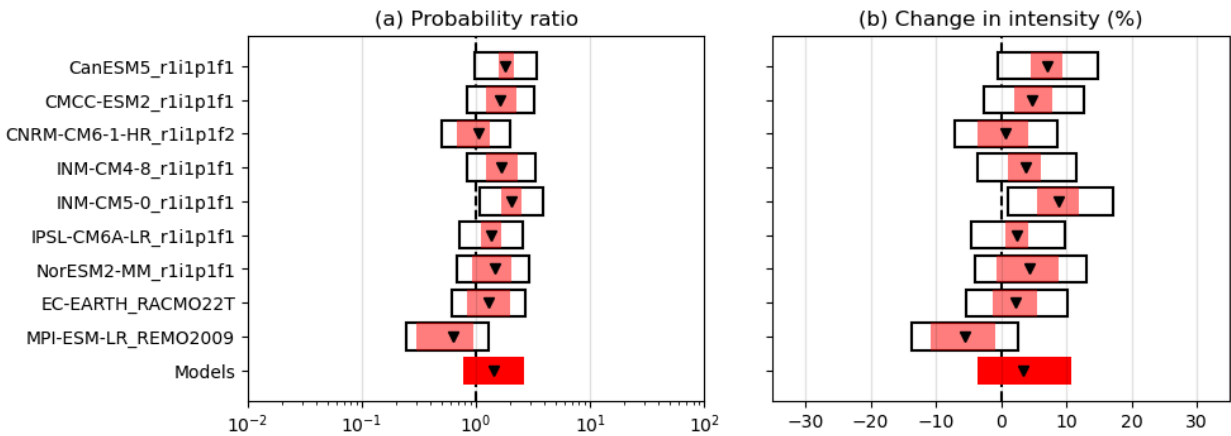


Figure 6.2: Synthesis of (a) probability ratios and (b) relative intensity changes of RX30day over the study region in the 2023 climate and a 0.8°C warmer climate, for all models that were judged ‘reasonable’ or ‘good’ in the model evaluation step. Details of how to interpret the synthesis plots are given in the text.

While we cannot follow the usual WWA protocol to combine observations and models into an overarching attribution statement, these results indicate that the observed increase in the last 15 years is at least in part driven by anthropogenic climate change and thus should be expected to continue to intensify with future warming. This is furthermore consistent with what is expected in a warming climate through the Clausius-Clapeyron relationship, which predicts more rainfall during the kind of short, intense episodes that characterise the MAM rainy season ([O’Gorman, 2015](#)).

7 Vulnerability and exposure

Reviewing the factors that drive vulnerability and exposure (V&E) is crucial for understanding the impacts of the 2024 MAM floods in Kenya, Tanzania, and Burundi. The floods, characterised by intense

and prolonged rainfall, triggered cascading hazards such as landslides and soil saturation, severely impacting communities already grappling with the losses and damages from previous extreme weather events. The timing of these floods, following the OND floods and coinciding with Cyclone Hidaya, has strained response resources, diminished adaptive capacities, and eroded infrastructure.

Natural hazards, including extreme rainfall and drought, are increasing in frequency and intensity in the region ([Kimutai et al., 2023](#)), compounding impacts and increasing the vulnerability of individuals reliant on weather-dependent livelihoods ([Weingärtner et al., 2022](#); [Thalheimer et al., 2023](#)). Beyond pastoralists, older adults (older women in particular) and the poor, marginalised, displaced and facing homelessness, are disproportionately affected ([Omolo & Mafongoya, 2019](#); [Bezgrebelna et al., 2023](#); [Walters & Gaillard, 2014](#)). Floods can also be drivers of poverty, as a poverty trap is created when people and communities with limited financial means face barriers to adequately recover from (compounding) economic disruptions, losses, and damages ([Sherwood, 2013](#)).

7.1 Land use management

In Kenya, Tanzania, and Burundi, there have been changes in land use and land cover over the past decades that likely had an impact on flood risks.

In Kenya, a drastic reduction in forest cover has been observed over the past two decades, with a 14% average decline from 2002 to 2022, and up to 39% in areas like Narok ([Global Forest Watch, 2022a](#); [Umukiza et al., 2021](#)). The loss of forests, which have a high infiltration rate (89.1 cm/h), compared to agricultural land (15 cm/h) and rangeland (7.9 cm/h), has led to increased surface runoff and higher peak river discharges, from 167 m³/sec to 233 m³/sec, thus elevating flood risks ([Mireille et al., 2019](#); [Barasa & Perera, 2018](#)). Although Kenya has implemented a logging ban since 2018 and launched the REDD+ strategy to mitigate deforestation, the impact of these measures on reversing flood risks remains limited ([Natural Justice, 2023](#); [Republic of Kenya, 2020](#)). Kenya is currently implementing a tree cover plan of at least 30% by 2032 by growing 15 billion trees, with a target of 1 million trees annually ([MEFCC, 2024](#)).

Tanzania has similarly faced severe deforestation, losing approximately 19.4% of its forest cover between 1990 and 2010, amounting to around 8 million hectares ([Project Gaia, 2015](#)). The annual deforestation rate of 1%, driven by charcoal production, shifting cultivation, and rapid population growth, exacerbates the vulnerability to floods due to reduced land absorption capacity ([Tremblay & Lowry, 2016](#)). Studies indicate that the loss of vegetation cover and wetland degradation has led to increased peak flows and flood magnitudes, particularly in urban areas like Dar es Salaam ([Mzava et al., 2021](#); [Mfwango et al., 2022](#)). Despite Tanzania's participation in REDD+ and the implementation of sustainable forest management policies, deforestation continues due to inadequate inter-sectoral coordination and the socio-economic drivers, notably poverty and limited livelihood options, underlying land use changes ([Doggart et al., 2020](#); [Lund et al., 2016](#)).

Burundi presents a particularly acute case of deforestation, with only 6.6% of its original forest cover remaining as of 2022 ([Global Nature Fund, n.d.](#)). The country experienced the highest deforestation rates globally in the 1990s, driven by agricultural expansion, fuelwood collection, and civil conflict ([Ndanezerewe, 2022](#); [Hobbs & Knausenberger, 2003](#)). The conversion of hillsides and wetlands for

agriculture without proper erosion control has led to soil erosion and increased flood frequency ([World Bank, 2018](#)). Efforts to address deforestation, such as the national reforestation program and improved cooking stoves, are underway but are challenged by high population pressure and the need for sustainable livelihood alternatives ([UNEP, n.d.](#); [Global Nature Fund, n.d.](#)).

Overall, the increase in flood risk in these countries is closely linked to land use changes that have diminished natural vegetation cover and disrupted water retention functions. Effective mitigation requires comprehensive policies that integrate sustainable land management practices and address the socio-economic drivers of deforestation.

7.2 Urban planning and informality

East Africa has some of the fastest urbanisation rates worldwide ([African Development Bank, 2022](#)). During the current and widespread floods, every capital in Ethiopia, Somalia, Kenya, Tanzania and the economic capital in Burundi has been flooded, causing deaths, displacement, destruction of critical infrastructure and widespread concern of spreading infectious diseases ([The Guardian, 2024](#); [ECHO, 2024](#); [UN OCHA, 2024](#); [Arabnew, 2024](#); [Borkena, 2024](#); [Bloomberg, 2024](#)). All countries show stark increases in the number of people living in urban areas, with extremely high annual growth rates. Rapid and unplanned urbanisation often goes hand in hand with the formation of informal settlements, often in marginalised and hazard prone land, ([UN Habitat, 2023](#); [UN Habitat, 2023](#); [UN Habitat, 2023](#); [UN Habitat, 2023](#)), increasing the risk of floods turning into disasters. ([Raju, Boyd & Otto, 2022](#), [Alcantata-Ayala et al., 2022](#)) Informal settlements expand into hazard prone areas, as highlighted in Kibera, Mukuru, and Mathare in Nairobi, Kenya. In Kibera, more than 200.000 people live within 30 metre proximity to water bodies and in 2015 already more than 50% of Kibera residents were impacted by heavy precipitation ([UNFCCC, 2023](#); [Weingärtner et al., 2019](#); [Galvin & Maassen, 2021](#)). In Mukuru, houses along water-ways were demolished following a 48-hr evacuation order issued by the government in effort to prevent further deaths from flooding ([CitizenTV, 2024](#)). Populations in informal settlements throughout the study area are particularly vulnerable to flooding due to a combination of external factors such as inadequate road infrastructure, land tenure, housing infrastructure, access barriers to potable water services (proximity and cost), location (in flood-prone areas like riparian, wetlands etc), drainage systems, and limited access to health systems. A number of the most affected areas in this study are also located in marginalised land alongside urban rivers and flood evacuation channels that overflow ([New York Times, 2024](#); [Owour & Mwiturubani, 2021](#); [Zerbo, Deglgado & Gonzáles, 2020](#)). These spaces are often neglected and do not fall within formal governance structures. While neglect is what in part enables their existence, and tenuous or marginalised land tenure can help leave residents alone instead of evicted, the limited access to basic services often increases flood risk. For instance, an analysis of Bujumbura (Burundi), shows that some settlements of the city are lacking drainage systems, while existing older drainage systems are often clogged and not well-maintained ([Nsabimana et al., 2023](#)). Flooding in informal settlements can also have widespread impacts on business within informal settlements, often part of the informal economy and less protected from hazard shocks ([Satterthwaite et al., 2018](#)).

Dar es Salaam's geomorphology, a coastal city with four major rivers (Mpiji, Rufiji, Msimbazi, Kizinga and Mzinga) emptying into the Indian Ocean, makes it highly prone to flooding. March-April-May is the peak rainy season with flooding occurring on a near annual basis. The rapid, unplanned growth of the city

exacerbates flood risks, especially for those living on marginalised land in informal settlements. Solid waste management is another challenge in Dar es Salaam, as well as other cities in this study area, that leads to blocked drainage systems which further exacerbate flooding ([Sakijege & Dakyaga, 2022](#)).

Country differences are large, with 50.81% of the urban population living in informal settlements in Kenya, and 36.8% in Burundi ([Our World in Data, 2020](#)). While informal settlements are affected disproportionately, other parts of the different cities are also impacted. Businesses have been shut down or destroyed. Small scale businesses and many others are still recovering from the pandemic ([Schmid, Raju & Jensen, 2021](#)), making recovery from these floods potentially harder. Further, over 200 schools in Kenya and 200 classrooms in Burundi, as well as several health facilities, bridges and roads in multiple countries have been impacted ([Al Jazeera, 2024](#); [BBC, 2024](#); [UNOCHA, 2024](#)). Thus, repercussions will last long after the water disappears. As noted in an earlier attribution study on the area in 2023, multiple projects from state and non-state actors are ongoing in the region to reduce flood risks ([Kimutai et al., 2023](#)). However, despite urban planning efforts, financial constraints and challenges in effective project enforcement or execution frequently lead to failures ([World Bank, 2020](#)).

7.3 Disaster risk management

7.3.1 Flood protection

Flood protection infrastructure and interventions in Kenya, Tanzania, and Burundi demonstrate diverse approaches tailored to each country's unique challenges and resources.

In Kenya, the Kenya Water Security and Climate Resilience Program has significantly bolstered flood mitigation efforts, particularly in flood-prone counties such as Busia and Siaya. The National Water Storage Authority has commissioned various flood control projects (like building of dykes) along major rivers prone to floods to improve the drainage capability of various rivers and impound the flow within the floodplain and river channels ([NWSA, 2024](#)). Additionally, Flood Control International has introduced advanced flood prevention measures, including flood barriers, gates, and doors, to protect critical infrastructure like airports and water treatment plants ([Flood Control International, n.d.](#)). Regular clean-up campaigns across informal settlements further help to clear drains and avert blockages that could precipitate flooding ([Gullet, 2016](#)).

Tanzania has employed a range of structural interventions to mitigate flood risks. The installation of gabions and concrete blocks along major rivers like the Mzase and Maswala has been crucial in preventing erosion ([Ministry of Transport, 2016](#)). River training and channel widening have enhanced water flow capacity, and parts of the Central Railway Line have been rerouted to circumvent flood-prone areas ([Ministry of Transport, 2016](#)). However, urban areas like Dar es Salaam still face significant flood management challenges due to rapid urbanisation, geomorphology and vulnerable informal settlements, necessitating ongoing improvements in infrastructure and urban planning ([Urban Agenda Platform, n.d.](#)). Tanzania also has a Disaster Management Act of 2015 which mandates the establishment of disaster management structures and delineates roles and responsibilities at national, regional/provincial, and local levels for disaster preparedness, early warning, response, and recovery activities related to all hazards, including floods ([IFRC, 2021](#)).

Burundi has adopted a comprehensive approach to flood risk management. The development of a multi-risk mapping and an online platform enables informed decision-making at various administrative levels ([IOM, 2023](#)). Large-scale infrastructure projects, such as the construction and rehabilitation of drainage systems, bridges, and dams, have been undertaken with active community involvement through cash-for-work programs ([IOM, 2023](#)). Moreover, innovative solutions like portable dams have been piloted in areas such as Mpanda Commune, offering dual benefits of flood protection and water storage ([UNEP, 2022](#)).

7.3.2 Early Warning Early Action

The intricate web of early warning systems (EWS) and anticipatory action mechanisms for floods in Kenya, Tanzania, and Burundi aims to mitigate impacts by enhancing preparedness and response capabilities. For example, the Regional Integrated Multi-Hazard Early Warning System for Africa and Asia (RIMES), an inter-governmental institution, provides services and capacity building for regional early warning for weather and climate extremes including flooding ([RIMES, n.d.-a](#); [RIMES, n.d.-b](#); [RIMES, n.d.-c](#)). The IGAD Climate Prediction and Applications Centre (ICPAC), based in Nairobi, also plays a pivotal role in providing weather and climate advisories for the region, supporting national initiatives ([Ambenje, 2004](#)). The IGAD Regional Roadmap for Anticipatory Action (IRRAA), launched in 2023, further harmonises these efforts by improving EWS and integrating early action principles across policies ([IGAD, 2023](#)). Moreover, responding to the several hazards and disasters faced by the continent, the African Union Commission (AUC) is developing the Africa Multi-Hazard Early Warning and Early Action System (AMHEWAS) Programme which is due for implementation by 2030 ([UNDP, 2023](#)).

In Kenya, the Kenya Meteorological Department (KMD) operates the National Flood Forecasting and Early Warning Centre (NFFEWC) ([Kiptum et al., 2023](#)). NFFEWC collects and monitors weather and climate data through observation networks across Kenya, and generates forecasts, early warnings, advisories, and alerts to relevant authorities as well as the public ([KMD, n.d.](#)). The Kenya Red Cross Society has developed an Early Action Protocol (EAP) for riverine flooding ([Anticipation Hub, 2021](#)). Anticipatory action includes cash grants, non-food item distribution, and emergency health and water services ([Anticipation Hub, 2023](#)). Additionally, Kenya's shock-responsive social protection systems, including the Hunger Safety Net Programme (HSNP), offer financial security to vulnerable populations during extreme weather events such as floods ([HSNP, 2023](#)).

Supported by the UK Meteorological Office, the Tanzania Meteorological Agency (TMA) has developed a Multi-Hazard Early Warning System (MHEWS) to provide early warnings for hazards including flooding. The MHEWS integrates advanced climate forecasting, local knowledge, and community engagement to improve flood prediction and response. This co-produced system enhances resilience and preparedness by providing timely, accessible (e.g. by color-coding and using pictorial symbols), and impact-based warnings to relevant government agencies and the public ([Roux et al., 2019](#), [WISER, 2017](#)).

Kenya and Tanzania's Developing Risk Awareness through Joint Action (DARAJA) system provides flood warnings tailored for informal urban settlements in Nairobi and Dar es Salaam, emphasizing community involvement and user-centric information dissemination through SMS and public campaigns ([UNDRR, n.d.](#); [World Habitat Awards, 2024](#)). Since 2018, when it launched, DARAJA has provided improved weather information to about one million people across the two countries ([Resurgence, 2024](#)).

Based on the information, communities have undertaken early actions including repairing roofs and homes (300% and 122% increases in Nairobi and Dar es Salaam, respectively), cleaning community and household drains, and moving possessions to places with less flood risk ([World Habitat Awards, 2024](#); [Resurgence, 2024](#)). For reference, while there are no definitive figures, it is estimated that 50-70% of Nairobi's (equal to over 2 million people) and up to 75% of Dar es Salaam's (equal to nearly 5 million people) populations reside in informal settlements ([Ren et al., 2020](#)). Thus, this innovative approach has made strides to protecting vulnerable residents, however they remain limited. There is an equally urgent need to address the underlying challenges of growing informal settlements that expand into hazard-prone areas. For example, in Dar es Salaam, informality is spreading into flood-prone areas, such as Msasani Bonde la Mpunga ([Kemwita et al., 2022](#)).

The flood EWS in Burundi, overseen by the National Meteorological and Hydrological Services (BHMD), includes two 24-hour synoptic stations, 19 climatological stations, 125 rainfall measurement sites, and five automatic weather stations (AWS) ([Ntibasharira, n.d.](#)). Ensuring continuous weather monitoring nationwide, BHMD provides hydrological modeling, weather forecasts, and early warnings ([Ntibasharira, n.d.](#)). The CREWS East Africa Initiative and IOM's efforts to develop multi-hazard early warning systems further strengthen Burundi's capacity to respond to flood risks ([UNDRR, 2023](#); [IOM, 2024](#)). In Burundi, the EAP for floods, supported by the World Food Programme (WFP) and the Burundi Red Cross, was activated in October 2023, enabling anticipatory measures such as cash distributions based on extreme rainfall forecasts ([Anticipation Hub, n.d.](#)).

Collectively, these initiatives illustrate a growing emphasis on proactive disaster management, leveraging forecasting, community engagement, and coordinated response strategies to mitigate flood impacts across East Africa. Still, city-level EWS for primary and secondary cities could significantly help improve the protection of growing urban populations by providing localised real-time weather information that takes into account the diverse, dense, and dynamic character of cities ([ELLA, n.d.](#); [Ramalingam & Clarke, 2012](#)). It is important to note that as the climate continues to warm, frequent and intense extreme events, including flood-inducing rainfall will exacerbate vulnerability and dampen adaptive capacity of many vulnerable communities across the region. Countries here have been caught in a cycle of debt and crisis that seems nearly impossible to escape as current national financial frameworks and public budgets cannot meet the scale of finance required to support the confluence of crises. Furthermore, over the past few years countries have had to pay more to service record levels of debt; more than one in five emerging markets and developing countries paid more to service their debt in 2022 than they received in external financing. This could rise to more than one in three by 2025 ([ONE Campaign, 2024](#)). Even with timely early warnings, adequate preparedness and response capabilities (e.g. evacuation to safer and higher ground) might be limited. Still, financing for climate adaptation is quite uneven and inadequate across the world; representing only a small fraction of what is needed, e.g., in Africa ([Trisos et al., 2022](#); [Savvidou et al., 2021](#)).

7.3.3 Emergency response

The 2024 floods in Kenya, Tanzania, and Burundi have prompted extensive emergency response efforts from both governmental and non-governmental organizations. In Kenya, the government established multi-agency emergency response centers in Nairobi to monitor the flood situation, deploy coordinated responses, and issue daily alerts ([Oruta, 2024](#)). This initiative includes evacuating residents from high-risk

areas, and providing emergency housing and food assistance. Moreover, the government has already allocated funding for infrastructure reconstruction ([Al Jazeera, 2024](#)). The International Organization for Migration (IOM), supported by the Government of Japan, is delivering shelter and essential items to 39,000 affected individuals in the most severely impacted regions ([IOM, 2024](#)). The KRCS has deployed Red Cross Action and Community Disaster Response teams to affected counties for search, rescue, and emergency relief operations, including the provision of shelter, food, and clean water. Amid increased needs due to heavy rains, KRCS, coordinating with governments, has activated contingency plans to aid 500,000 people, prioritizing vulnerable households across 42 counties ([IFRC, 2024](#)). In certain areas, response efforts have been hindered by the destruction of critical infrastructure such as roads, airstrips, and bridges ([IFRC, 2024a](#)).

In Tanzania, the government has deployed search and rescue services, conducted damage assessments, and provided comprehensive support, including healthcare, food, water, sanitation, and hygiene ([IFRC, 2024b](#); [UNICEF, 2024](#)). By April 21, 2024, 2,882 individuals across five camps had received humanitarian aid by the government and various humanitarian partners, including food staples and non-food items like bedding, mosquito nets, and tents. Additional support encompassed mental health services, education, and child protection ([OCHA, 2024](#)).

In Burundi, the government has raised the harbour protection wall to protect Bujumbura's port and launched construction projects to safeguard critical infrastructure ([Manishatse, 2024](#)). Coordination with UN agencies and the Burundi Red Cross Society (BRCS) has been integral. IOM's efforts include providing emergency shelter, blankets, and other essentials to over 5,000 people and supporting their relocation to safer areas ([IOM, 2024](#)). Together with IOM, the BRCS has conducted disability monitoring. It has moreover distributed tents to 100 households in Cibitoke and identified 250 in Bujumbura for rental support. Volunteers conducted epidemic control, reaching 1,350 people. Hygiene awareness reached 1,080 households, with 540 sprayed. WASH kits aided 150 households in Bujumbura ([IFRC, 2024c](#)).

V&E conclusions

Recurring disasters in East Africa threaten the region's efforts in ensuring sustainable development. In the past few years, countries in this region have dealt with the COVID-19 pandemic, as well as multiple back-to-back flood, and drought episodes, straining their capacity and resources to respond effectively.

The analysis of drivers of flood risks and impacts in Kenya, Tanzania, and Burundi reveals the critical role of land use management, urban planning, adaptation and disaster risk management. In these East African nations, deforestation and agricultural expansion have significantly increased flood risks. For instance, Kenya's 14% forest cover reduction has heightened surface runoff and peak river discharges, exacerbating flood hazards. Similarly, Tanzania's 19.4% forest loss, driven by charcoal production and shifting cultivation, reduces land absorption capacity, while Burundi's severe deforestation from agricultural expansion and civil conflict leads to soil erosion and frequent floods. Comprehensive policies integrating sustainable land management practices and addressing socio-economic drivers of deforestation are crucial for mitigating these flood risks.

Urbanisation compounds these risks, as rapid and unplanned growth in cities like Nairobi and Dar es Salaam results in vulnerable informal settlements lacking adequate infrastructure, increasing flood susceptibility. The recurrent flooding in capital cities demonstrates the pressing need for improved urban planning and resilient infrastructure. There are efforts to mitigate these risks including Kenya's flood barriers and clean-up campaigns, Tanzania's river training and structural interventions, and Burundi's comprehensive flood management projects. Despite these measures, financial constraints and coordination issues persist, undermining effectiveness. Effective urban planning, improved infrastructure, and targeted interventions in informal settlements are essential for reducing the impact of floods on vulnerable urban populations.

Data availability

All time series used in this analysis are available via the Climate Explorer.

References

All references are given as hyperlinks in the text.

Acknowledgements

Joyce Kimutai, Emmanuel Raju, Friederike Otto and Nick Baumgart are part of the project- “Climate Change Attribution and Vulnerability in Kenya” with funding from the Ministry of Foreign Affairs, Denmark. (DFC File No. 23-12-KU)

Appendix - additional plots

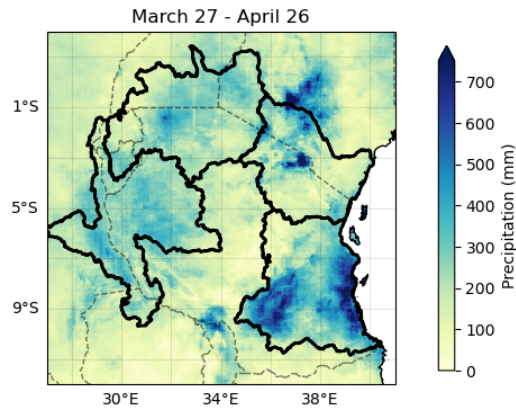


Figure A1: Subregions used to check the spatial persistence of the East Africa Paradox. Clockwise from bottom left: Lake Tanganyika basin; Lake Victoria basin; Central Highlands & river catchments; southeastern Tanzania.

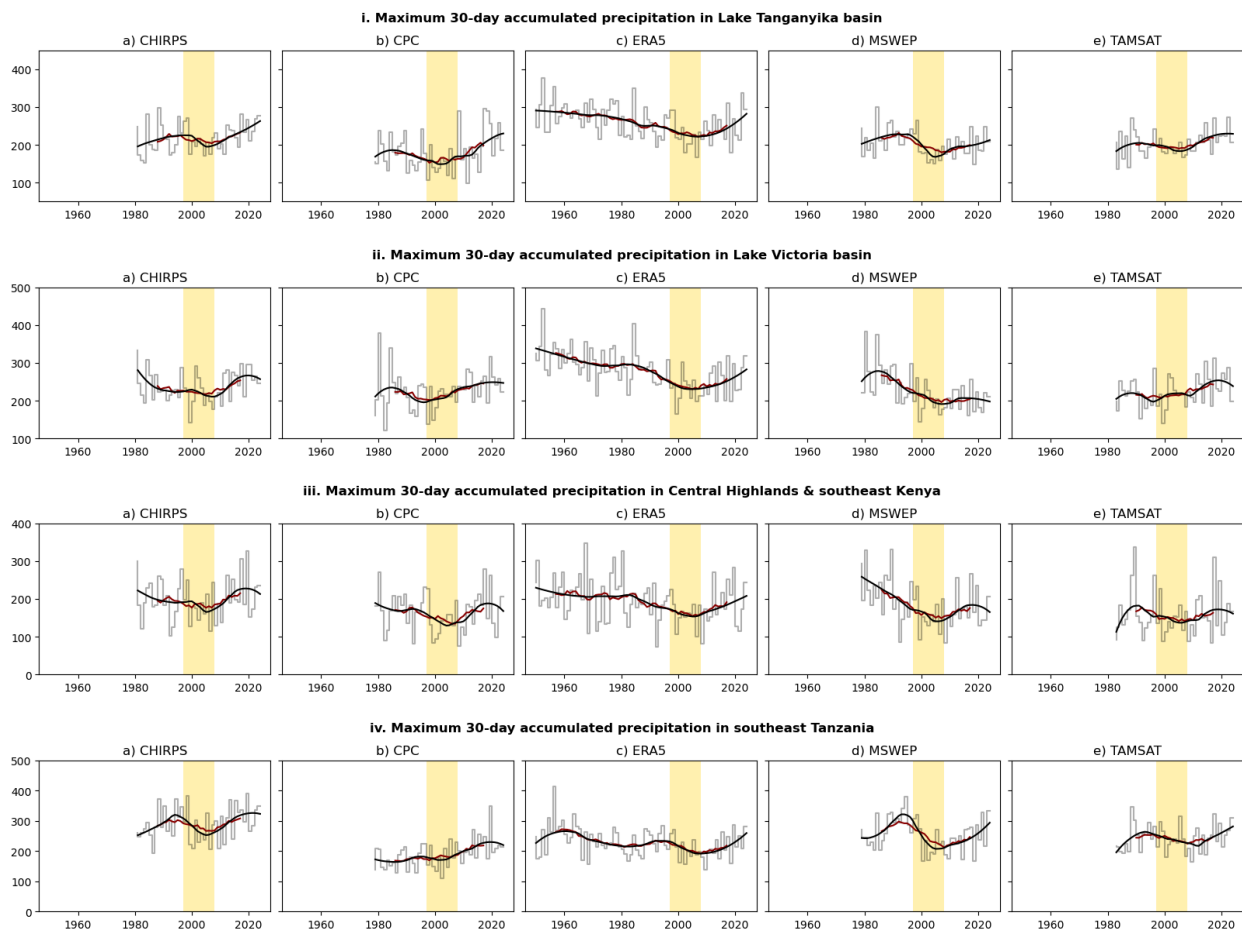


Figure A2: Time series of MAM RX30day over the study region in the four sub-regions defined in Figure A1, in five gridded data products. The thick black line is a loess (local regression) curve; the dark red line is a 15-year rolling mean. The shaded region indicates the period from 1997-2008.

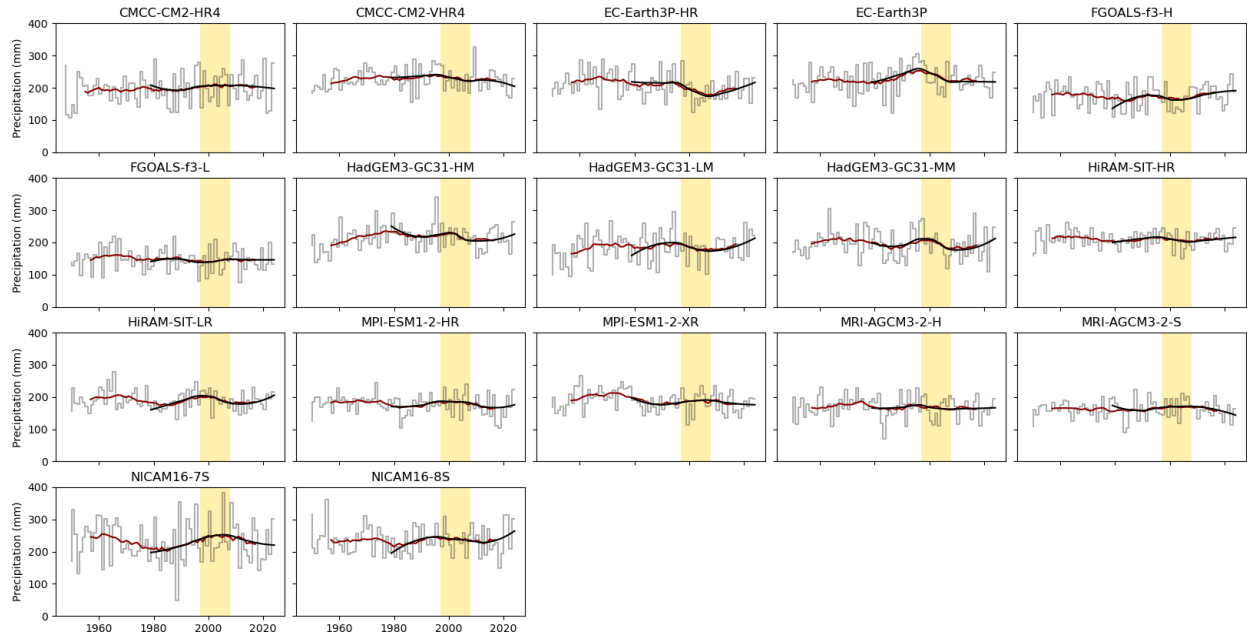


Figure A3: Time series of MAM RX30day over the study region in seventeen HighResMIP runs. The thick black line is a loess (local regression) curve fitted to the period covered by the observed time series (1979-2024); the red line is a 15-year running mean. The shaded region indicates the period from 1997-2008.

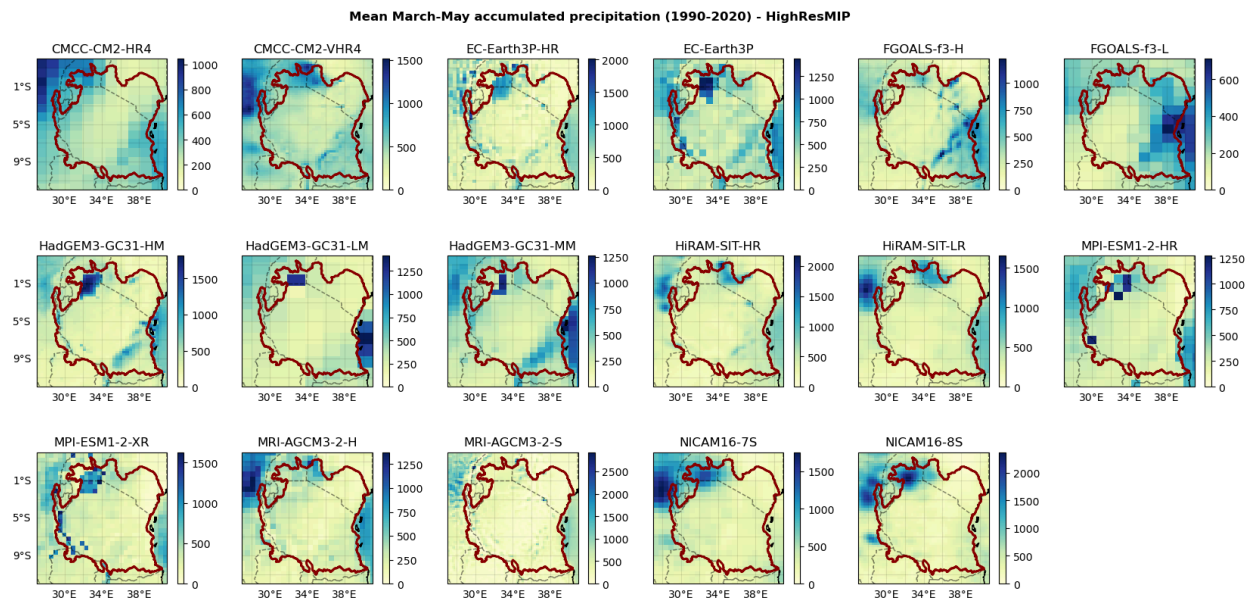


Figure A4: MAM climatology (mean accumulated precipitation) from 1990-2020 in HighResMIP models. The study region is outlined in red.

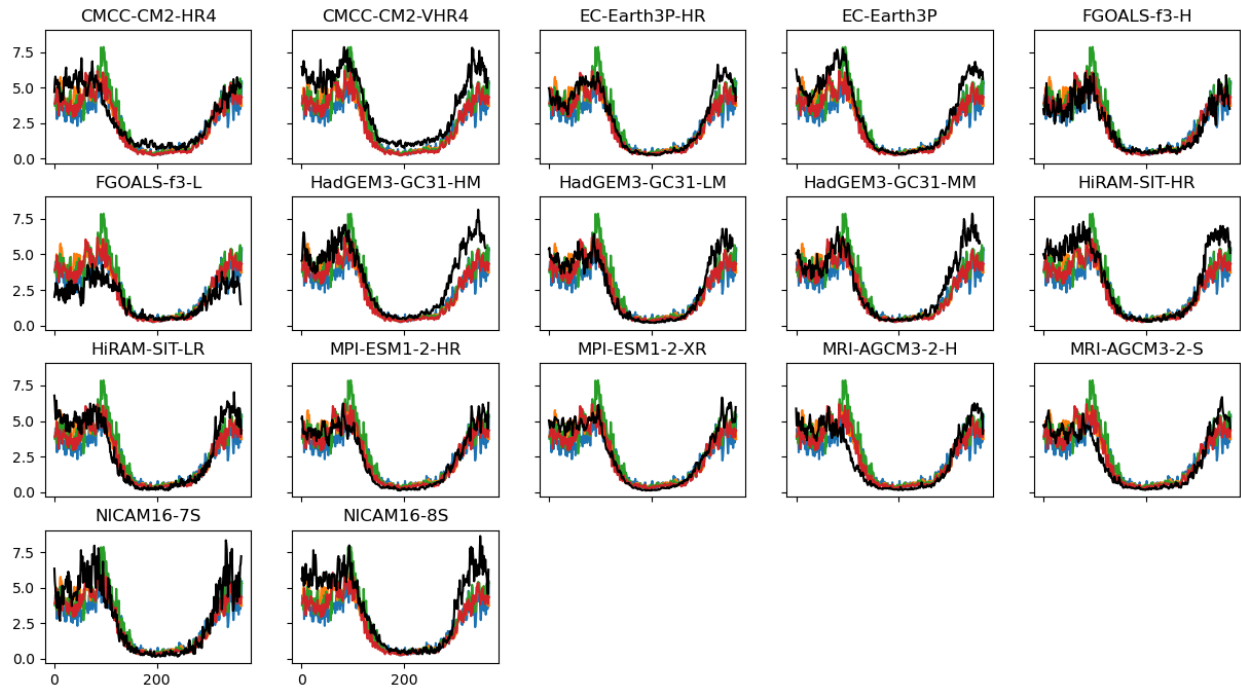


Figure A5: Seasonal cycle of mean precipitation over the study region from 1990-2020 in HighResMIP models (black line) vs gridded observational products: CPC (blue); CHIRPS (green); MSWEP (orange); TAMSAT (red).

Seasonal MAM average PR 1991-2020 (mm/season)

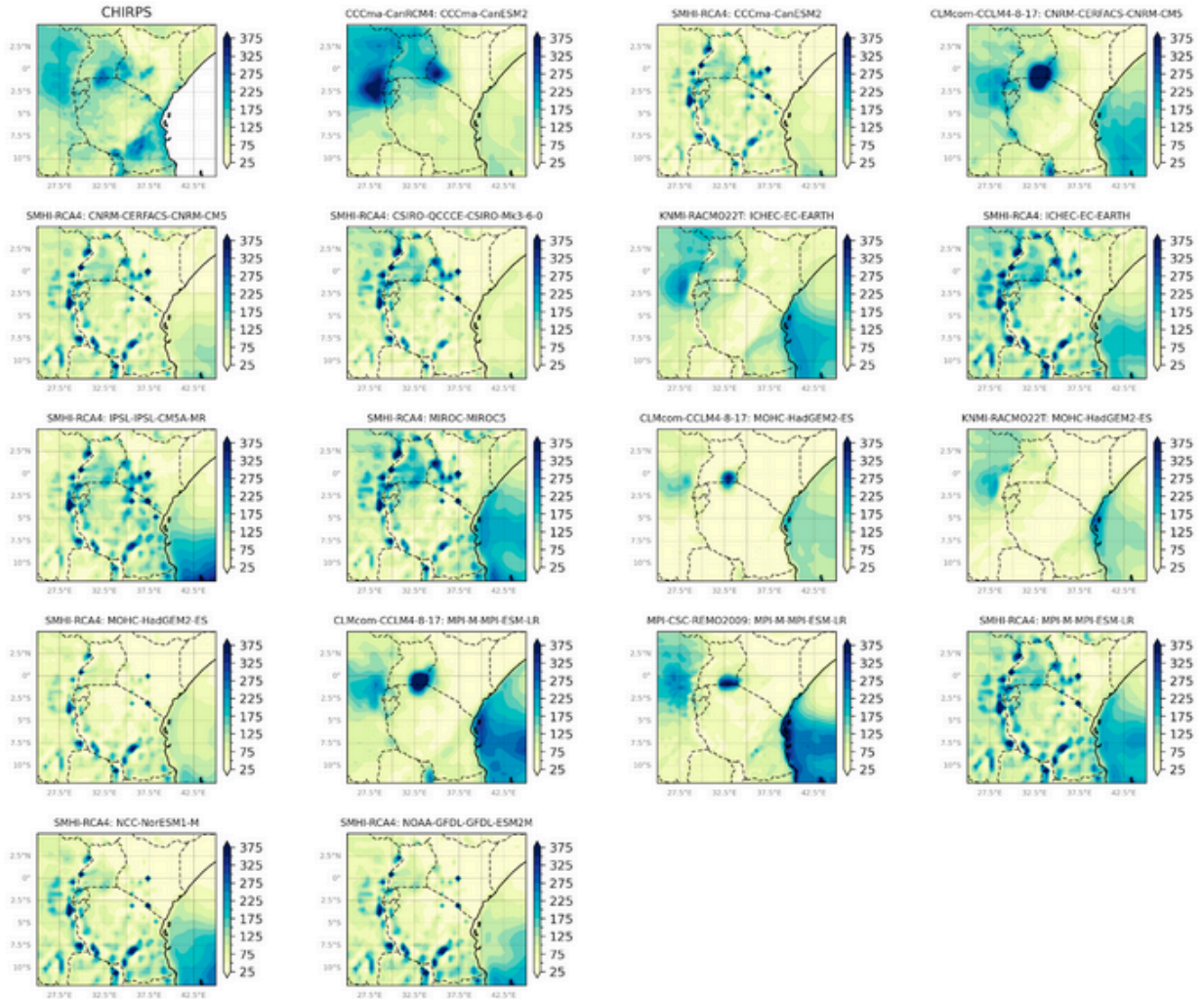


Figure A6: MAM climatology (mean accumulated precipitation) from 1990-2020 in CORDEX runs.

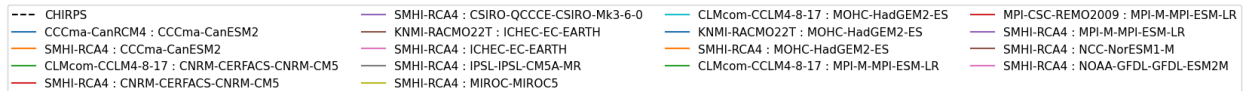
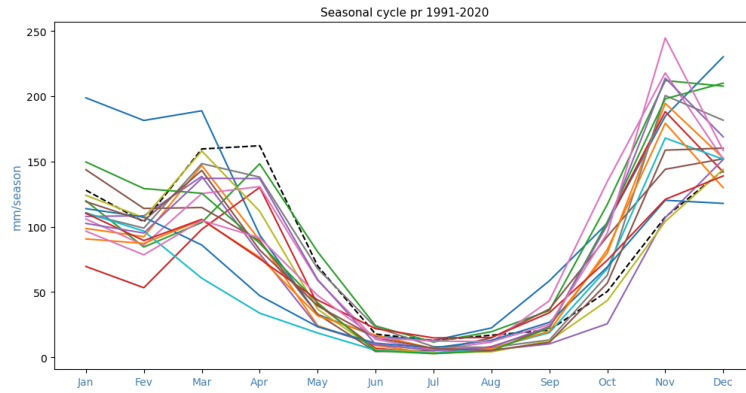


Figure A7: Seasonal cycle of mean precipitation over the study region from 1990-2020 in CORDEX runs (coloured lines) vs CHIRPS (black dashed line).

Mean March-May accumulated precipitation (1990-2020) - CMIP6

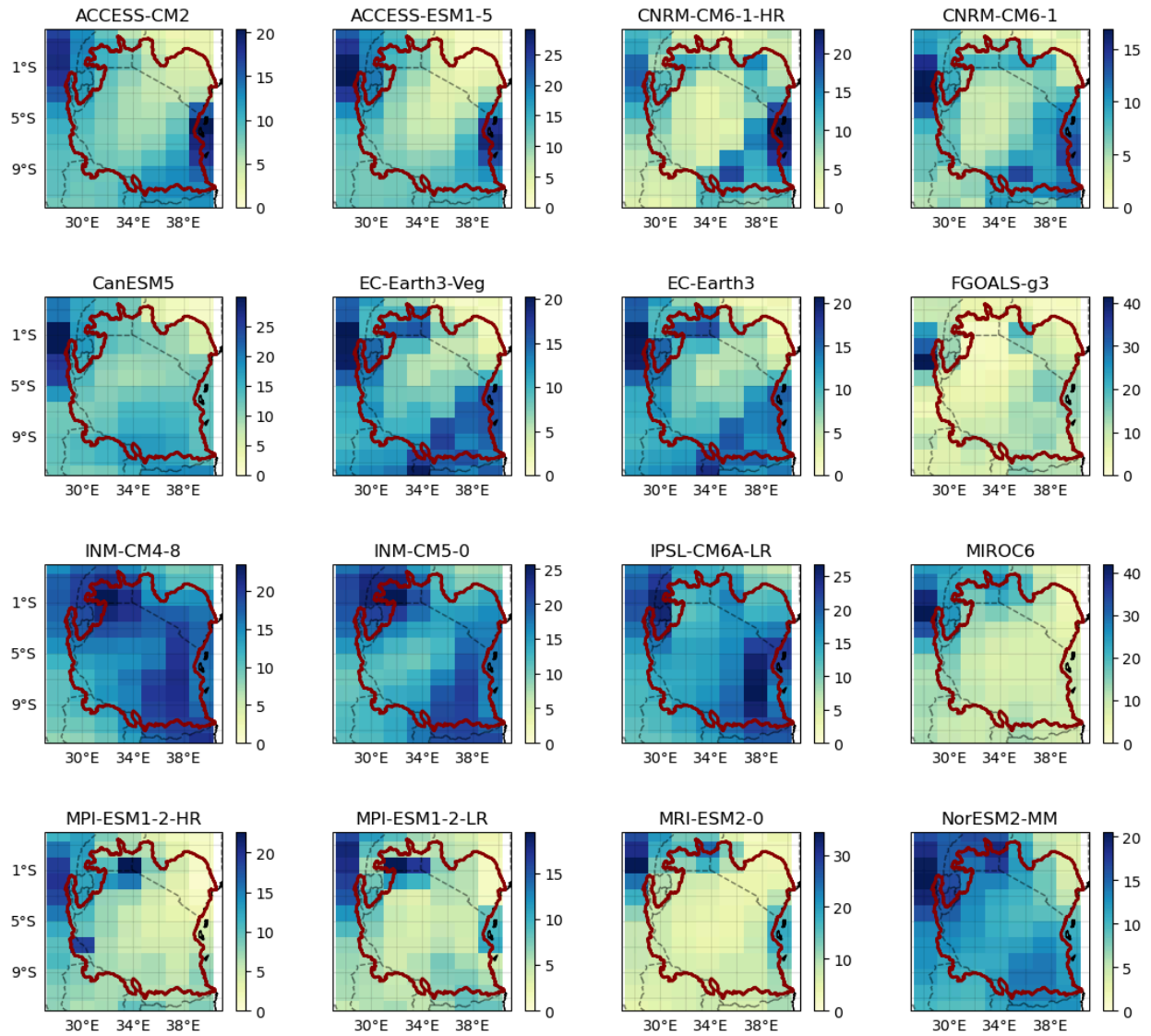


Figure A8: MAM climatology (mean accumulated precipitation per day) from 1990-2020 in CMIP6 models. The study region is outlined in red.

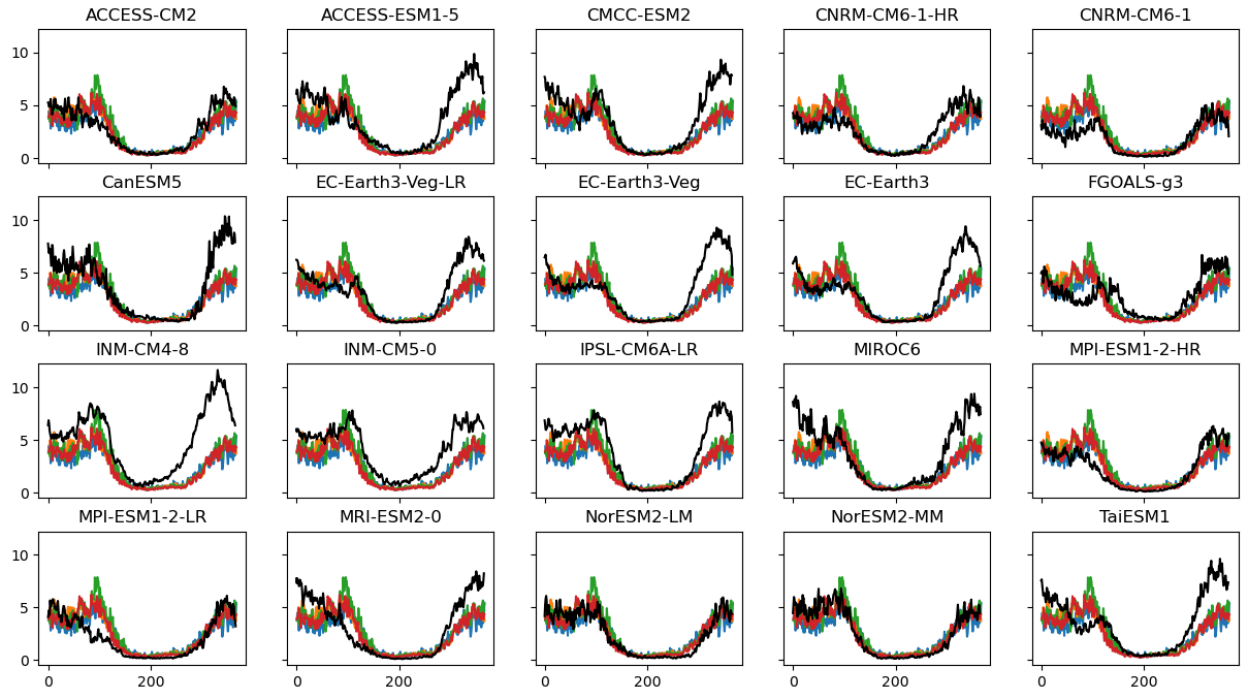


Figure A9: Seasonal cycle of mean precipitation over the study region from 1990-2020 in HighResMIP models (black line) vs gridded observational products: CPC (blue); CHIRPS (green); MSWEP (orange); TAMSAT (red).

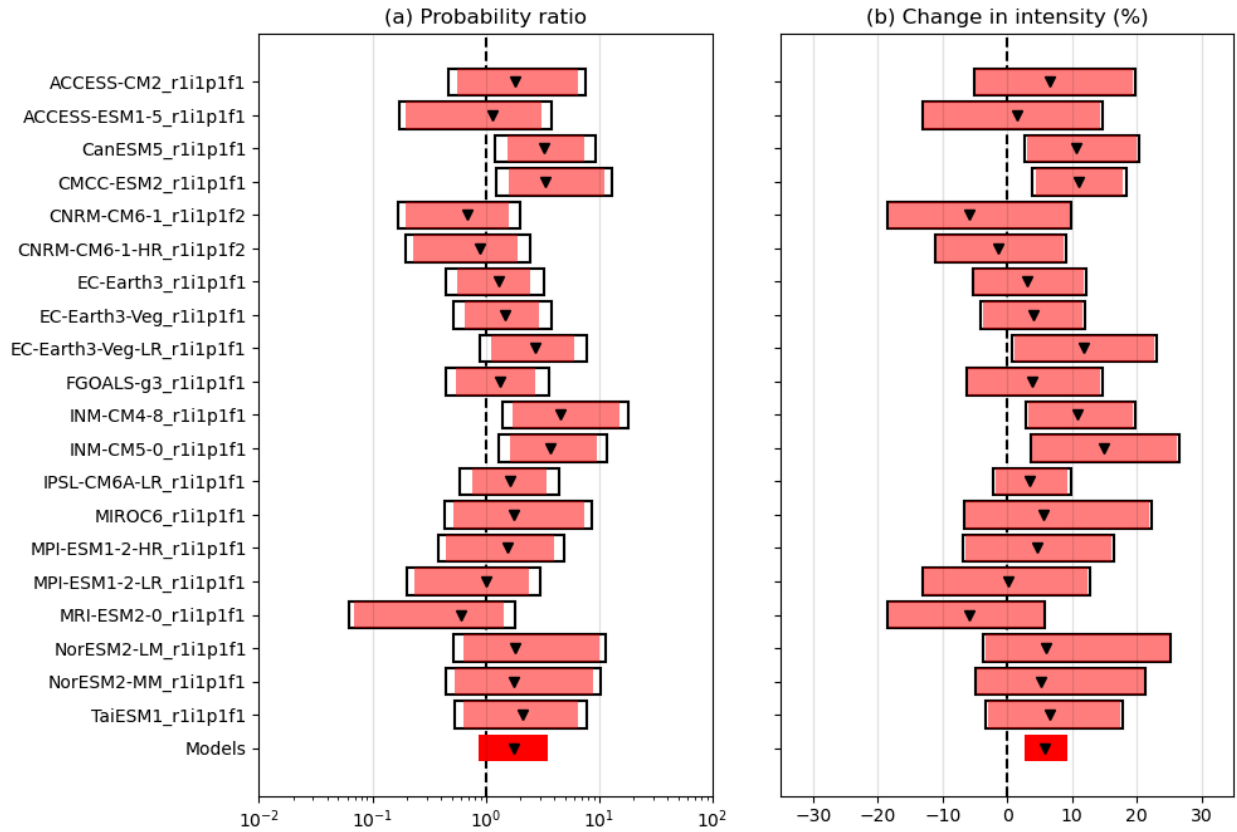


Figure A10: Synthesis of (a) probability ratios and (b) relative intensity changes of *RX30day* over the study region in the 2024 climate and a 1.2°C cooler climate, for twenty CMIP6 model runs regardless of the evaluation results. Details of how to interpret the synthesis plots are given in the text.